**Computers and Concrete**, *Vol. 19, No. 2 (2017) 171-177*
DOI: https://doi.org/10.12989/cac.2017.19.2.171


# Estimating of water pressure to avoid hydraulic fracturing in water pressure test

Hassan Bakhshandeh Amnieh[*1] and Majid Masoudi[2a]

[1]*School of Mining, College of Engineering, University of Tehran, Iran*
[2]*Department of Mining Engineering, Faculty of Engineering, University of Kashan, Iran*

*(Received September 9, 2016, Revised November 20, 2016, Accepted November 21, 2016)*

**Abstract.** Water pressure test operation is used before the grouting to determine the rate of penetrability, the necessity and estimations related to grouting, by the penetration of water into the borehole. One of the parameters which have the highest effect is pressure of water penetration since the application of excessive pressure causes the hydraulic fracture to occur in the rock mass, and on the other hand, it must not be so small that prevents from seeing mechanical weaknesses and the rate of permeability. Mathematical modeling is used for the first time in this study to determine the optimum pressure. Thus, the joints that exist in the rock mass are simulated using cylindrical shell model. The joint surroundings are also modeled through Pasternak environment. To obtain equations governing the joints and the surroundings, energy method is used accompanied by Hamilton principle and an analytical solution method is used to obtain the maximum pressure. In order to validate the modeling, the pressure values obtained by the model were used in the sites of Seymareh and Aghbolagh dams and the relative error rates were measured considering the differences between calculated and actual pressures. Modeling in the sections of Seymareh dam showed 4.75, 3.93, 4.8 percent error rates and in the sections of Aghbolagh dam it rendered the values of 22.43, 5.22, 2.6 percent. The results indicate that this modeling can be used to estimate the amount of pressure for hydraulic fracture in water pressure test, to predict it and to prevent it.

**Keywords:** water pressure test; hydraulic fracture; mathematical modeling; cylindrical shell model

## 1. Introduction

Generally, grouting operation, is one of the ways to reduce water leakage, increase strength and consolidate jointed rock on the sites (Economides 1990). To determine the permeability of jointed rocks, in situ tests are usually used two of which are applied more frequently: water pumping test (Lugeon) and borehole filling tests (Lefranc) (Wong and Farmer 1993). In the water pumping test which is usually called Water Pressure Test (WPT), water is penetrated at a certain section of the borehole under a variable pressure. However, in the filling with water test, water enters the rock through the walls or the bottom of the borehole, but this takes place only under the pressure of the water column in the borehole (Rice 1998).

Lugeon conducted the first water pressure test in 1933. The results of his tests have been the most common and best means of hydraulic evaluation for grouting in rock masses till now (Garagash 2003). Despite its shortcomings, this test is one of the few methods that contain all the scientific and engineering aspects mentioned before.

Absorption of one liter of water per minute for each meter of the borehole at the pressure of one mega Pascal is equal to one lugeon: 1 LU=1lit.min$^{-1}$.m$^{-1}$ (Van Dam 1999).

Lugeon number is always between one and 100 and if this value is higher than 100, it is considered to be 100

$$LU=10Q/Pe \quad (1)$$

Where $Q$ is the quantity of the water absorbed in liters per meter per minute, $Pe$ is the highest effective pressure in the test and $LU$ is the lugeon value. One of the most important issues that must be investigated and prevented in the water pressure test is known as hydraulic fracturing (Van de Ketterij 2001). As can be seen in Fig. 1, when hydraulic fracturing happens, high pressure causes the rock mass to break. The dilation phenomenon through which the fractures present in the rock, open due to high pressure is sometimes called hydraulic jacking, too (Wang 2009).

However, it must be noted that conducting hydraulic fracture tests is absolutely essential to understand the fracturing behavior in the rock mass but such tests must be performed in a controlled manner since in most cases, the permeability of the waste caused by hydraulic fracturing is high. In order to separate these two states, pressure and flow rates must be continuously recorded (Lhomme 2005). Fig. 2 shows the continuous recording of pressure and flow for hydrofracturing and jacking test.

Different types of stones, geological structures and in situ stress affect fracturing behavior and jacking in the rock mass. Therefore, the maximum pressure of the test will be also influenced by these factors (Tolppanen 2003). The foundation of dams is damaged by fracturing and jacking. Thus, the maximum pressure must not cause fracturing and

∗Corresponding author, Associate Professor
E-mail: hbakhshandeh@ut.ac.ir
[a]Ph.D. Student
E-mail: masoudi@staff.kashanu.ac.ir



ISSN: 1598-8198 (Print), 1598-818X (Online)

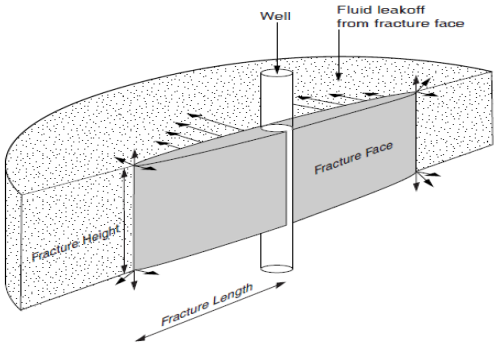


Fig. 1 Water penetration and hydraulic fracturing in rock mass (Creager 1997)

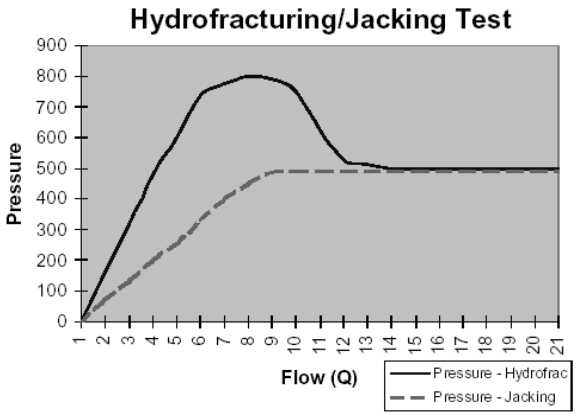


Fig. 2 The relationship between pressure and flow in hydro fracturing and jacking test (Mack 1994)

jacking in the rock mass (Tolppanen 2003).

However, pressure must not be so low that prevents us from observing mechanical weaknesses. Critical pressure has a wide range. In weak rocks, very low pressures (for example, 5 bar), can cause fracturing regardless of the depth. In strong rocks, a high pressure is required to fracture the rock even in shallow depth. Generally, critical pressure is independent of depth (El Tani 2012).

Water pressure test can determine the rate of permeability and the necessity of grouting and estimate the rate of sealing resulted from grouting. It must be noted that in some sites there are rocks in which the recorded water take is low but the grout take is high. The reason for this is the fracturing of the rock mass due to high pressure in grouting (Yew and Weng 2014). Therefore, it can be seen that the hydraulic fracturing phenomenon can take place in both water test and grouting operations and thus it is very important to investigate this phenomenon and try to prevent its occurrence (Wang 2009).

In this research mathematical modeling is used for the first time to determine the optimum pressure. Thus, the joints that exist in the rock mass are simulated using cylindrical shell model. The joint surroundings are also modeled through Pasternak environment. Elastic buckling of a thin cylindrical shell was studied by Karam *et al.* (1995), Agrawal and Sobel (1997) investigated the weight compressions of cylindrical shells with various stiffness under axial compression. Buckling of cylindrical shells with metal foam cores was presented by Hutchinson and He

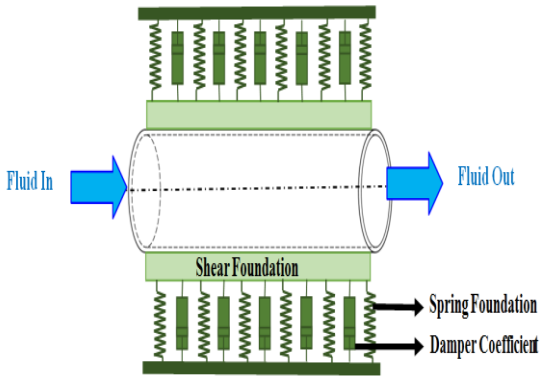


Fig. 3 A schematic figure of embedded cylindrical shell

(2000), Elastic stability of cylindrical shell with an elastic core under axial compression was investigated by Arani *et al.* (2007) using energy method. Ye *et al.* (2011), however, investigated bucking of a thin-walled cylindrical shell with foam core under axial compression. Junger and Mass (1952) studied coupled vibrations of fluid-filled cylindrical shell based on shear shell theory and discussed the free vibration of orthotropic cylindrical shells filled partially or completely with an incompressible, non-viscous fluid. The static instability of a nanobeam with geometrical imperfections imperfections embedded in elastic foundation was investigated by Mohammadi *et al.* (2014), Using semi-analytical finite strip method, the buckling behavior of laminated composite deep as well as thick shell of revolution under follower forces which remain normal to the shell was investigated by Khayat *et al.* (2016).

With respect to development works on buckling of the cylindrical shell, it should be noted that none of the research mentioned above, have considered smart composite and their specific characteristic. Micromechanical modeling which has the potential to take into account the electrical load was used by Tan and Tong (2011) for studying an imperfect textile composite. However, neither the matrix nor the reinforced piezoelectric polymetric composites subjected to combined electro-thermo-mechanical loading were investigated by Salehi-Khojin and Jalili (2008), Arani *et al.* (2011) carried out a stress analysis in cylinder and spheres made from piezoelectric materials using analytical method.

## 2. Mathematical modeling

A schematic diagram, of a cylindrical shell is shown in Fig. 3 in which geometrical parameters of length, $L$, radius, $R$ and thickness $h$ are also indicated. The surrounding foundation is simulated with spring and shear constants.

### *2.1 Stress-strain relations*

Shear strains $\gamma xz$, $\gamma\theta z$ are considered negligible in the Kirchhoff deformation theory. Hence, the tangential displacements $u$, $v$ become linear function of the radial coordinate ($z$) (Arani *et al.* 2011). In other words

$$\begin{aligned} v(x,\theta,z) &= v(x,\theta) - z\frac{\partial w(x,\theta)}{\partial \theta}, \\ w(x,\theta,z) &= w(x,\theta). \\ u(x,\theta,z) &= u(x,\theta) - z\frac{\partial w(x,\theta)}{\partial x}, \end{aligned} \tag{2}$$

The strain components $\bar{\varepsilon}_{xx}$, $\bar{\varepsilon}_{\theta\theta}$ and $\bar{\gamma}_{x\theta}$ at an arbitrary point of the shell are related to the middle surface strains $\varepsilon xx$, $\varepsilon\theta\theta$ and $\gamma x\theta$ and to the changes in the curvature and torsion of the middle surface $kxx$, $k\theta\theta$ and $kx\theta$ by the following relationships

$$\begin{Bmatrix} \overline{\varepsilon_{xx}} \\ \overline{\varepsilon_{\theta\theta}} \\ 2\overline{\varepsilon_{x\theta}} \end{Bmatrix} = \begin{Bmatrix} \varepsilon_{xx} \\ \varepsilon_{\theta\theta} \\ \gamma_{x\theta} \end{Bmatrix} - z\begin{Bmatrix} k_{xx} \\ k_{\theta\theta} \\ k_{x\theta} \end{Bmatrix} = \left( \begin{bmatrix} \frac{\partial}{\partial x} \\ 0 \\ \frac{\partial}{2R\partial\theta} \end{bmatrix} \right.$$

$$\left. \begin{bmatrix} 0 & 0 \\ \frac{\partial}{R\partial\theta} & \frac{1}{R} \\ \frac{\partial}{2\partial x} & 0 \end{bmatrix} - z\begin{bmatrix} 0 & 0 & \frac{\partial^2}{\partial x^2} \\ 0 & 0 & \frac{\partial^2}{R^2\partial\theta^2} \\ 0 & 0 & 2\frac{\partial^2 w}{R\partial x\partial\theta} \end{bmatrix} \right) \times \begin{bmatrix} u \\ v \\ w \end{bmatrix}, \tag{3}$$

Where $u$, $v$ and $w$, describe the displacements in the orthogonal coordinate system $x$, $\theta$, $z$ established at the middle surface of the shell.

Using Hook law, the constitutive equation may expressed follows (GhorbanpourArani 2011)

$$\begin{Bmatrix} \sigma_{xx} \\ \sigma_{\theta\theta} \\ \sigma_{x\theta} \end{Bmatrix} = \begin{bmatrix} C_{11} & C_{12} & 0 \\ C_{12} & C_{22} & 0 \\ 0 & 0 & C_{66} \end{bmatrix} \left[ \begin{Bmatrix} \frac{\partial u}{\partial x} \\ \frac{\partial v}{R\partial\theta} + \frac{w}{R} \\ \frac{\partial u}{R\partial\theta} + \frac{\partial v}{\partial x} \end{Bmatrix} - z\begin{Bmatrix} \frac{\partial^2 w}{\partial x^2} \\ \frac{\partial^2 w}{R^2\partial\theta^2} \\ 2\frac{\partial^2 w}{R\partial x\partial\theta} \end{Bmatrix} \right], \tag{4}$$

Where $\sigma_{ij}$ ($i$, $j$=$x$, $\theta$) stresses as well as $u$, $v$, $w$ are the displacements of a arbitrary point of the shell in the axial, circumferential and radial directions, respectively. Also, $C_{ij}$, $i$, $j$=1,…6), correspond to elastic constants.

### *2.2 Energy method*

The total potential energy of the pipe is the sumof strain energy, kinetic energy and work down by flowing fluid is expressed below where the strain energy is

$$\begin{aligned} U = \int_{-\frac{h}{2}}^{\frac{h}{2}} \iint_A \left( \sigma_{xx}\left( \frac{\partial u}{\partial x} - z\frac{\partial^2 w}{\partial x^2} \right) + \sigma_{\theta\theta}\left( \frac{\partial v}{R\partial\theta} + \frac{w}{R} + -z\frac{\partial^2 w}{R^2\partial\theta^2} \right) \right. \\ \left. + \sigma_{x\theta}\left( \frac{\partial u}{R\partial\theta} + \frac{\partial v}{\partial x} - 2z\frac{\partial^2 w}{R\partial\theta\partial x} \right) \right) dz\, dA, \end{aligned} \tag{5}$$

And the kinetic energy is

$$K = \frac{\rho}{2}\int_v \left( (\frac{\partial u}{\partial t})^2 + (\frac{\partial v}{\partial t})^2 + (\frac{\partial w}{\partial t})^2 \right) dV, \tag{6}$$

And the work down by internal viscose fluid is (Wang and Ni 2009)

$$\begin{aligned} W = \int (F_{fluid}) w dA = \int \left( -h\rho_f \left( \frac{\partial^2 w}{\partial t^2} + 2v_x \frac{\partial^2 w}{\partial x \partial t} + v_x{}^2 \frac{\partial^2 w}{\partial x^2} \right) \right. \\ \left. + h\mu \left( \frac{\partial^3 w}{\partial x^2 \partial t} + \frac{\partial^3 w}{R^2 \partial \theta^2 \partial t} + v_x \left( \frac{\partial^3 w}{\partial x^3} + \frac{\partial^3 w}{R^2 \partial \theta^2 \partial x} \right) \right) \right) w dA. \end{aligned} \tag{7}$$

Now replacing these in the following expression based on the Hamilton principal

$$\int_0^t (\delta K - \delta U + \delta W) dt = 0, \tag{8}$$

And defining the following non-dimensional quantities

$$\begin{aligned} &\{\bar{u}, \bar{v}, \bar{w}\} = \frac{\{u, v, w\}}{h}, \quad \gamma = \frac{h}{l}, \quad \xi = \frac{x}{l}, \quad \beta = \frac{h}{R}, \quad \bar{C}_{ij} = \frac{C_{ij}}{C_{11}}, \\ &\bar{\rho} = \frac{\rho_s}{\rho_f}, \quad \mu = \frac{\mu_0}{h\sqrt{C_{11}\rho_f}}, \quad V = v_x\sqrt{\frac{\rho_f}{C_{11}}}, \quad \bar{t} = \frac{t}{h\sqrt{\frac{\rho_f}{C_{11}}}}, \end{aligned} \tag{9}$$

The four electro-thermo mechanical coupling governing equations of PVDF cylindrical shell conveying viscose fluid, can therefore be written as

$$\begin{aligned} &\gamma^2\left( \frac{\partial^2 \bar{u}}{\partial \xi^2} + \frac{\partial \bar{w}}{\partial \xi}\frac{\partial^2 \bar{w}}{\partial \xi^2} \right) + \gamma\beta\bar{C}_{12}\left( \frac{\partial^2 \bar{v}}{\partial \xi \partial \theta} \cdot \right. \\ &\left. + \frac{\partial \bar{w}}{\partial \xi} + \beta_s \frac{\partial \bar{w}}{\partial \theta}\frac{\partial^2 \bar{w}}{\partial \xi \partial \theta} \right) + \beta\bar{C}_{66}\left( \beta\frac{\partial^2 \bar{u}}{\partial \theta^2} + \frac{\partial^2 \bar{v}}{\partial \xi \partial \theta} \right. \\ &\left. + \beta\frac{\partial \bar{w}}{\partial \xi}\frac{\partial^2 \bar{w}}{\partial \theta^2} + \frac{\partial \bar{w}}{\partial \xi} + \beta\frac{\partial \bar{w}}{\partial \theta}\frac{\partial^2 \bar{w}}{\partial \xi \partial \theta} \right) + \gamma^2 \bar{e}_{11}\frac{\partial^2 \Phi}{\partial \xi^2} = (\bar{\rho})\frac{\partial^2 \bar{u}}{\partial \bar{t}^2}, \end{aligned} \tag{10}$$

$$\begin{aligned} &\beta\bar{C}_{12}\left( \frac{\partial^2 \bar{u}}{\partial \xi \partial \theta} + \frac{\partial \bar{w}}{\partial \xi}\frac{\partial^2 \bar{w}}{\partial \xi \partial \theta} \right) + \beta^2\bar{C}_{22}\left( \frac{\partial^2 \bar{v}}{\partial \theta^2} \right. \\ &\left. + \frac{\partial \bar{w}}{\partial \theta} + \beta\frac{\partial \bar{w}}{\partial \theta}\frac{\partial^2 \bar{w}}{\partial \theta^2} \right) + \gamma\bar{C}_{66}\left( \frac{\beta\partial^2 \bar{u}}{\partial \xi \partial \theta} + \frac{\partial^2 \bar{v}}{\partial \xi^2} \right. \\ &\left. + \frac{\beta\partial^2 \bar{w}}{\partial \theta \partial \xi}\frac{\partial \bar{w}}{\partial \xi} + \frac{\beta\partial \bar{w}}{\partial \theta}\frac{\partial^2 \bar{w}}{\partial \xi^2} \right) + \beta\bar{e}_{12}\frac{\partial^2 \Phi}{\partial \xi \partial \theta} = \bar{\rho}\frac{\partial^2 \bar{v}}{\partial \bar{t}^2}, \end{aligned} \tag{11}$$

$$\begin{aligned} &\frac{\gamma^2}{12}\left( -\gamma^2\frac{\partial^4 \bar{w}}{\partial \xi^4} - \bar{C}_{12}\beta^2\frac{\partial^4 \bar{w}}{\partial \xi^2 \partial \theta^2} \right) + \frac{1}{12} \\ &\left( -\gamma^2\beta^2\bar{C}_{12}\frac{\partial^4 \bar{w}}{\partial \xi^2 \partial \theta^2} - \beta^4\bar{C}_{22}\frac{\partial^4 \bar{w}}{\partial \theta^4} \right) \\ &-\frac{\gamma\beta\bar{C}_{12}}{3}\left( \frac{\partial \bar{u}}{\partial \xi} + \frac{\gamma}{2}\left( \frac{\partial \bar{w}}{\partial \xi} \right)^2 \right) - \beta\bar{C}_{22} \end{aligned} \tag{12}$$

Table 1 A list of input data in modeling

| Row | Name of the input parameter | Value of the input parameter |
|---|---|---|
| 1 | Dimensions of the given rock | 1×1 |
| 2 | Density of the rock | 2.7 grams per cubic centimeter |
| 3 | Joint break (*b*) | 1 mm |
| 4 | Elasticity module | 1130 kg/m$^3$ |
| 5 | Shear stiffness coefficient | $10^9$ |
| 6 | Poisson coefficient | 0.3 |
| 7 | Grout penetration range | 46.5 cm |
| 8 | Borehole radius | 3.5 cm |

$$\left(\frac{\partial \bar{v}}{\partial \theta}+\beta \bar{w}+\frac{\beta^2}{2}\left(\frac{\partial \bar{w}}{\partial \theta}\right)^2\right)- \\ -\left[\frac{\partial^2 \bar{w}}{\partial \bar{t}^2}+2\gamma V\frac{\partial^2 \bar{w}}{\partial \xi \partial \bar{t}}+\gamma^2 V^2\frac{\partial^2 \bar{w}}{\partial \xi^2}\right] \\ -\mu\left[\gamma^2\frac{\partial^3 \bar{w}}{\partial \xi^2 \partial \bar{t}}+V\gamma^3\frac{\partial^3 \bar{w}}{\partial \xi^3}+\beta^2\left(\frac{\partial^3 \bar{w}}{\partial \theta^2 \partial \bar{t}}\right.\right. \\ \left.\left.+V\gamma\frac{\partial^3 \bar{w}}{\partial \theta^2 \partial \xi}\right)\right]+\gamma\beta\bar{e}_{12}\frac{\partial \Phi}{\partial \xi}=\bar{\rho}\frac{\partial^2 \bar{w}}{\partial \bar{t}^2}, \quad (12)$$

### 2.3 Navier method

Considering simply supported boundary condition, the mechanical displacement may be written as

$$u(x,\theta)=u_0\cos(\frac{n\pi x}{L})\sin(m\theta), \quad (13)$$

$$v(x,\theta)=v_0\sin(\frac{n\pi x}{L})\cos(m\theta), \quad (14)$$

$$w(x,\theta)=w_0\sin(\frac{n\pi x}{L})\sin(m\theta), \quad (15)$$

Substituting Eq. (9) into Eqs. (6)-(8) results

$$\begin{bmatrix} K_{11} & K_{12} & K_{13} \\ K_{21} & K_{22} & K_{23} \\ K_{31} & K_{32} & K_{33} \end{bmatrix}\begin{bmatrix} u_0 \\ v_0 \\ w_0 \end{bmatrix}=0, \quad (16)$$

Solving the above equation, the displacement may be obtained. However, using the obtained displacement and Eq. (7), the pressure of fluid can be calculated.

## 3. Modeling details

In the mathematical model, the parameters shown in Table 1 were inserted into the modeling as the input data.

## 4. Case study

Table 2 An instance of the results of water pressure test and grouting in some boreholes of the Seymareh dam

| Data obtained from P-22 borehole | | | | | Data obtained from P-20 borehole | | | | |
|---|---|---|---|---|---|---|---|---|---|
| Number of section | Depth (m) | LU | P(pa) | V(m3) | Number of section | Depth (m) | LU | P(pa) | V(m3) |
| 1 | 0-5 | 11.4 | 233000 | 0.021625 | 1 | 0-5 | 3.8 | 230000 | 0.012667 |
| 2 | 5-10 | 41.5 | 376000 | 0.032417 | 2 | 5-10 | 2.7 | 377000 | 0.012667 |
| 3 | 10-15 | 20.5 | 523000 | 0.068458 | 3 | 10-15 | 22.4 | 523000 | 0.0095 |
| 4 | 15-20 | 39.4 | 764000 | 7.291667 | 4 | 15-20 | 69.9 | 552000 | 5.216667 |
| 5 | 20-25 | <1 | 964000 | 0.154208 | 5 | 20-25 | <1 | 974000 | 0.015833 |
| 6 | 25-30 | 3.1 | 1162000 | 0.106833 | 6 | 25-30 | 22.8 | 1029000 | 7.654167 |
| 7 | 30-35 | 7 | 1299000 | 0.097375 | 7 | 30-35 | 1.34 | 1247000 | 0.025333 |
| 8 | 35-40 | <1 | 1587000 | 0.005375 | 8 | 35-40 | <1 | 1456000 | 0.022167 |
| 9 | 40-45 | <1 | 1794000 | 0.010792 | 9 | 40-45 | <1 | 1639000 | 0.019 |
| 10 | 45-50 | 6.4 | 2230000 | 0.022167 | 10 | 45-50 | <1 | 2064000 | 0.015833 |
| 11 | 50-53 | 18.5 | 2082000 | 0.256125 | 11 | 50-53 | 19.54 | 1886000 | 2.6665 |
| Data obtained from P-19 borehole | | | | | Data obtained from P-23 borehole | | | | |
| Number of section | Depth (m) | LU | P(pa) | V(m3) | Number of section | Depth (m) | LU | P(pa) | V(m3) |
| 1 | 0-5 | 54.3 | 130000 | 0.012667 | 1 | 0-5 | 51.3 | 225000 | 0.172625 |
| 2 | 5-10 | 29.8 | 377000 | 0.012667 | 2 | 5-10 | 72.2 | 343000 | 0.123333 |
| 3 | 10-15 | 10.9 | 521000 | 5.291667 | 3 | 10-15 | 10.3 | 522000 | 0.026667 |
| 4 | 15-20 | 6.7 | 695000 | 8.691667 | 4 | 15-20 | 5 | 767000 | 0.019458 |
| 5 | 20-25 | 11.54 | 1015000 | 0.006333 | 5 | 20-25 | 4.1 | 795000 | 0.049417 |
| 6 | 25-30 | 26.9 | 1066000 | 0.012667 | 6 | 25-30 | 95 | 1037000 | 3.110833 |
| 7 | 30-35 | 2.2 | 1291000 | 0.038 | 7 | 30-35 | 6.1 | 1207000 | 0.074667 |
| 8 | 35-40 | 4.5 | 1682000 | 0.022167 | 8 | 35-40 | 1.82 | 1445000 | 0.127667 |
| 9 | 40-45 | <1 | 1743000 | 0.022167 | 9 | 40-45 | <1 | 1663000 | 0.004833 |
| 10 | 45-50 | 3.6 | 3980000 | 0.019 | 10 | 45-50 | 3.8 | 2074000 | 0.021083 |
| 11 | 50-53 | 11.2 | 2381000 | 0.025325 | 11 | 50-53 | 18.2 | 2232000 | 3.98665 |

### 4.1 Seymareh dam

Seymareh dam and its power plant are located in Iran, 40 km northwest of Dareshahr city and 7.5 km away from Cheshme Shirin village in Ilam province. Its purpose is to use the potential power in Seymareh river. Seymareh is a thin double-arched concrete dam with the height of 130 m from the present river bed (and about 180 m from the bedrock). Dam crest elevation is 730 m and at the normal elevation, water level is at the 720 m height above high sea level. The length of the dam crest at the elevated part of the dam crest is 202 m. The capacity of the dam reservoir is 3.215 billion cubic meters. In Table 2, some results of water take and cement grout in the boreholes P-19, P-20, P-22 and P-23 in this dam are shown.

### 4.2 Aghbolagh dam

Aghbolagh earth dam is located at the distance of 32 km in the south of Borujen city in Chahar Mahal-o-Bakhtiari province in Iran. The geographical coordinates of the dam axis in the UTM system are *x*=520363 and *y*=3512353.

Table 3 Some results of the water pressure test and grouting in some boreholes of the Aghbolagh dam

| Borehole name | Depth | LU | Cement take (kg) |
|---|---|---|---|
| TG-1 | 4-6 | 100 | 134 |
| | 6-10 | 100 | 242 |
| | 10-15 | 14 | 151 |
| | 15-20 | 25 | 536 |
| | 20-25 | 1 | 114 |
| | 25-30 | 2 | 1175 |
| | 30-35 | 2 | 1325 |
| | 35-40 | 1 | 627 |
| | 40-45 | 26 | 3335 |
| Borehole name | Depth | LU | Cement take (kg) |
| TG-2 | 4-7/3 | 100 | 573 |
| | 7/3-12 | 12 | 486 |
| | 12-17 | 49 | 133 |
| | 17-22 | 100 | 1971 |
| | 22-27 | 1 | 44 |
| | 27-32 | 1 | 38 |
| | 32-45 | 2 | 2466 |
| Borehole name | Depth | LU | Cement take (kg) |
| TG-3 | 4/2-5/8 | 100 | 462 |
| | 5/8-8/3 | 100 | 201 |
| | 8/3-13 | 37 | 104 |
| | 18-23 | 1 | 38 |
| | 23-28 | 1 | 33 |
| | 28-33 | 1 | not injection |
| | 33-38 | 1 | not injection |
| | 38-43 | 1 | not injection |
| | 43-45 | 1 | not injection |

Considering the geological map, the area under study is located in the Zagros zone and under the Overthrust zone.

From the stratigraphic perspective, Mesozoic and Cenozoic rocks, especially the Cretaceous rocks are dominant in this zone and from the structural point of view, large faults such as the main Zagros fault and Dena fault play a major role in the zone. In Table 3, some results of water take and cement grout in the boreholes TG-1, TG-2 and TG-3 in this site are shown.

## 5. Results of modeling

In this section, based on the results obtained from the water pressure test in Seymareh and Aghbolagh dams and comparison of the real pressure values with the calculated pressure acquired through modeling, the results achieved by modeling were validated. The resulting consists of water pressure values in the some sections that hydraulic fracturing has occurred. These data are shown in Table 4. In Fig. 4, the amount of convergence among these values is shown.

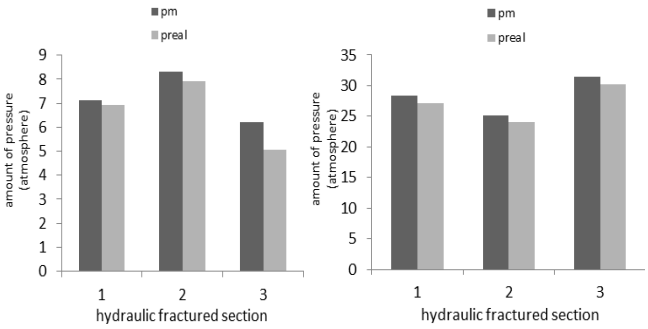


(a) (b)

Fig. 4 convergence rate between calculated fracturing pressure ($P_m$) and real fracturing pressure ($P_{real}$) in (a) Aghbolagh and (b) Seymareh dams

Table 4 Comparison between water pressures that result in hydraulic fracturing in water pressure test and the calculated fracturing pressure in atmosphere

| Aghbolagh dam | | Seymareh dam | |
|---|---|---|---|
| Calculated pressure | Real pressure | Calculated pressure | Real pressure |
| 7.121 | 6.94 | 28.421 | 27.13 |
| 8.323 | 7.91 | 25.174 | 24.02 |
| 6.195 | 5.06 | 31.387 | 30.2 |

Table 5 Values of relative error between calculated fracturing pressures and real pressures in percentage

| Aghbolagh dam | Seymareh dam |
|---|---|
| 2.6 | 4.75 |
| 5.22 | 4.8 |
| 22.43 | 3.93 |

## 6. Comparison and analysis of the results

According to the results shown in Fig. 4, it can be seen that there is a high degree of convergence between the values of the real recorded pressure in Seymareh and Aghbolagh dams and the values measured through modeling. In order to validate the modeling, relative error of the measured pressure ($P_m$) was compared to the real recorded pressure (Preal) obtained from the $E=((P_{real}-P_m)/P_{\text{real}})\times 100$. The results are shown in Table 5.

The results shown in Tables 4 and 5 and Fig. 4, indicate that there is desirable correlation between calculated fracturing pressure and the fracturing pressure recorded in Seymareh and Aghbolagh dam sites. This shows that the proposed model has desirable precision in predicting and estimating the rate of hydraulic fracturing.

The aim of this study is analysis of the water pressure in the water pressure test in order to prevent the occurrence of hydraulic fracturing in the rock mass. This is so because hydraulic fracturing not only prevents us from achieving the goal of determining permeability rate in the rock mass but also causes damage to the site and deteriorates the quality of the rock mass. Therefore, estimating the rate of water pressure which causes fractures is highly important. To do

so, mathematical modeling and simulation of the joint conditions was conducted using a cylindrical shell and the pressure causing fracture was calculated. In order to validate the results, real values of hydraulic fracturing pressure recorded in operations in Seymareh and Aghbolagh dams were used and the processes of change in real pressure values and calculated pressure values were controlled. The results showed that there is desirable convergence and correlation between these two sets of values. In addition, calculation of the relative error between them in Seymareh dam showed 4.75, 3.93, 4.8 percent error rates and in the sections of Aghbolagh dam it rendered the values of 22.43, 5.22, 2.6 percent. The results indicate that mathematical modeling can be used to predict the occurrence of the hydraulic fracturing phenomenon and thus preventing it from happening.

## 7. Conclusions

What is examined in this study is Analysis the rate of water pressure that is penetrated in water pressure test to prevent the phenomenon of hydraulic fracturing in rock mass. Not only does the occurrence of hydraulic fracturing prevents us from achieving the goals of this test, namely seeing mechanical weaknesses and the rate of the site's permeability, but also causes most of the joints to open, creates fractures in the rock mass and deteriorates its quality. Therefore, estimating the rate of water pressure which causes fractures is highly important. To do so, mathematical modeling and simulation of the joint conditions was conducted using a cylindrical shell and the pressure causing fracture was calculated. In order to validate the results, real values of hydraulic fracturing pressure recorded in water pressure test in Seymareh and Aghbolagh dams were used and the processes of change in real pressure values and calculated pressure values were controlled.

• The results showed that there is desirable convergence and correlation between these two sets of values.

• Calculation of the relative error between them showed that the mathematical model in the sections of the Seymareh dam under study had the error values of 4.75, 3.93 and 4.8 percent.

• In the Aghbolagh dam sections, the error values were equal to 22.43, 5.22 and 2.6 percent.

• These results indicate that mathematical modeling can be used to predict the occurrence of hydraulic fracturing phenomenon in water pressure test operations and thus increase the efficiency and productivity of such processes.

## References


Arani, A.G., Kolahchi, R. and Barzoki, A.M. (2011), "Effect of material in-homogeneity on electro-thermo-mechanical behaviors of functionally graded piezoelectric rotating shaft", *Appl. Math. Model.*, **35**(6), 2771-2789.

Cleary, M.P., Johnson, D.E., Kogsbøll, H.H., Owens, K.A., Perry, K.F., De Pater, C.J. and Mauro, T. (1993), "Field implementation of proppant slugs to avoid premature screen-out of hydraulic fractures with adequate proppant concentration in low permeability reservoirs symposium", *Proceedings of the Low Permeability Reservoirs Symposium*, Society of Petroleum Engineers, Colorado, U.S.A., April.

Creager, M. and Paris, P.C. (1997), "Elastic field equations for blunt cracks with reference to stress corrosion cracking", *J. Fract. Mech.*, **3**(4), 247-252.

Economides, M.J. (1990), "Implications of cementing on well performance", *Develop. Petrol. Sci.*, **28**, 1.

El Tani, M. (2012), "Grouting rock fractures with cement grout", *Rock Mech. Rock Eng.*, **45**(4), 547-561.

Fett, T. (1999), "Estimated stress intensity factors for semi-elliptical cracks in front of narrow circular notches", *Eng. Fract. Mech.*, **64**(3), 357-362.

Garagash, D.I. (2003), "Evolution of a plane-strain fracture driven by a power-law fluid", *Proceedings of the 16th ASCE Engineering Mechanics Conference*, Seattle, U.S.A., July.

Gulrajani, S.N., Nolte, K.G. and Romero, J. (1997), "Evaluation of the M-Site B-sand fracture experiments: The evolution of a pressure analysis methodology", *Proceedings of the SPE Annual Technical Conference and Exhibition*, Texas, U.S.A., October.

Zhu, H.Y., Deng, J.G., Zhao, J., Zhao, H., Liu, H.L. and Wang, T. (2014), "Cementing failure of the casing-cement-rock interfaces during hydraulic fracturing", *Comput. Concrete*, **14**(1), 91-107.

Houlsby, A.C. (1990), *Construction and Design of Cement Grouting: A Guide to Grouting in Rock Foundations*, John Wiley & Sons.

Jafarian, A.A. and Kolahchi, R. (2016), "Buckling analysis of embedded concrete columns armed with carbon nanotubes", *Comput. Concrete*, **17**(5), 567-578.

Johnson, E. and Cleary, M.P. (1991), "Implications of recent laboratory experimental results for hydraulic fractures", *Proceedings of the Low Permeability Reservoirs Symposium*, Colorado, U.S.A., April.

Lhomme, T.P.Y. (2005), "Initiation of hydraulic fractures in natural sandstones", Ph.D. Dissertation, Delft University of Technology, The Netherlands.

Mack, M.G. and Elbel, J.L. (1994), "A simulator for modeling acid fracturing treatments".

Rice, J.R. (1998), "Mathematical analysis in the mechanics of fracture", *Fract.: Adv. Treat.*, **2**, 191-311.

Shroff, A.V. and Shah, D.L. (1999), "Grouting technology in tunnelling and dam construction", *A. A. Balkema*, **626**, 626.

Sneddon, I.N. and Transforms, F. (1991), *McGraw Hill Book Co. Inc.*, New York, U.S.A.

Tolppanen, P. and Syrjänen, P. (2003), *Hard Rock Tunnel Grouting Practice in Finland*, Sweden, and Norway-Literature Study by Finnish Tunnelling Association.

Van Dam, D.B. (1999), "The influence of inelastic rock behaviour on hydraulic fracture geometry", Ph.D. Dissertation, Delft University of Technology, The Netherlands.

Van de Ketterij, R.G. (2001), "Optimisation of the near-wellbore geometry of hydraulic fractures propagating from cased perforated completions", Ph.D. Dissertation, Delft University of Technology, The Netherlands.

Vinegar, H.J., Wills, P.B., DeMartini, D.C., Shlyapobersky, J., Deeg, W.F.J., Adair, R.G. and Sorrells, G.G. (1992), "Active and passive seismic imaging of a hydraulic fracture in diatomite", *J. Petrol. Technol.*, **44**(1), 28-90.

Wang, L. and Ni, Q. (2009), "A reappraisal of the computational modelling of carbon nanotubes conveying viscous fluid", *Mech. Res. Commun.*, **36**(7), 833-837.

Weijers, L. (1995), "The near-wellbore geometry of hydraulic fractures initiated from horizontal and deviated wells", Ph.D. Dissertation, Delft University of Technology, The Netherlands.

Wong, H.Y. and Farmer, I.W. (1993), "Hydrofracture mechanisms

in rock during pressure grouting", *Rock Mech.*, **5**(1), 21-41.
Yew, C.H. and Weng, X. (2014), *Mechanics of Hydraulic Fracturing*, Gulf Professional Publishing.

*CC*